applied sciences

MDPI

Article

Morphological Analysis of US Treated PANC-1 Spheroids

Martina Ricci *,†, Mattia Dimitri †, Martina Serio and Andrea Corvi

Department of Industrial Engineering (DIEF), University of Florence, Via di Santa Marta 3, 50139 Florence, Italy; mattia.dimitri@unifi.it (M.D.); martina.serio@edu.unifi.it (M.S.); andrea.corvi@unifi.it (A.C.)

* Correspondence: martina.ricci1@unifi.it; Tel.: +39-3311730200

† These authors contributed equally as last authors.

Abstract: This study investigates the impact of low-intensity continuous ultrasound (LICU) on pancreatic adenocarcinoma (PANC-1) spheroids, emphasizing morphological and volumetric transformations. PANC-1 spheroids were cultured and treated with LICU across frequencies from 1 to 5 MHz. Cell viability and mortality were analyzed through Calcein AM/PI staining, while volumetric and morphological changes were quantified across frequencies from 2 to 4 MHz using advanced imaging techniques and computational tools, including a custom Python OpenCv Library, AnaSP 3.0, a MATLAB based open source tool. Notably, a frequency of 3.5 MHz yielded optimal outcomes, also achieving a reduction in spheroid volume and mortality while minimizing disgregation, a factor linked to metastasis risk. These findings underscore LICU's potential as an effective therapeutic strategy, balancing tumor reduction with the preservation of structural cohesion. The study establishes a methodological framework for optimizing LICU parameters, presenting a less invasive avenue for improving therapeutic outcomes in pancreatic cancer treatment.

Keywords: LICU; volume evaluation; US cancer therapy; computer vision; spheroids disgregation; frequency induced mortality

Academic Editors: Sergio Castiñeira-Ibáñez, Constanza Rubio Michavila and Daniel Tarrazó-Serrano

Received: 30 December 2024
Revised: 30 January 2025
Accepted: 2 February 2025
Published: 7 February 2025

Citation: Ricci, M.; Dimitri, M.; Serio, M.; Corvi, A. Morphological Analysis of US Treated PANC-1 Spheroids. *Appl. Sci.* **2025**, *15*, 1707. https://doi.org/10.3390/app15041707

1. Introduction

Low-intensity continuous ultrasound (LICU) is gaining attention as a promising therapeutic strategy in oncology, particularly for treating challenging malignancies such as pancreatic ductal adenocarcinoma (PDAC). Unlike high-intensity focused ultrasound (HIFU), which relies on thermal ablation, LICU operates through non-thermal mechanisms, offering a fundamentally different approach to cancer treatment [1,2].

HIFU achieves tissue destruction by delivering high-intensity and high-voltage ultrasound waves to generate localized heating, resulting in thermal damage that ablates both cancerous and, potentially, adjacent healthy tissues [3–5]. In contrast, LICU uses significantly lower intensities that avoid thermal effects. Instead, it leverages pressure-related phenomena such as acoustic streaming and cavitation. Acoustic streaming refers to fluid motion induced by ultrasound waves, while cavitation involves the formation and oscillation of microbubbles within tissues [6,7].

Additionally, LICU has been associated with frequency-based resonance phenomena, a topic explored in recent studies [8]. Furthermore, LICU can also be associated with inhibition of tumor cell proliferation and enhancing anticancer drugs delivery through a phenomenon called sonoporation that enhances drug delivery through cell membranes [9–14].

Preliminary research [2,14–16] suggests that it can induce cytotoxic effects in cancer cells by disrupting their internal structures and communication networks. However,

its precise mechanisms of action remain under investigation, particularly regarding the interplay between pressure, frequency, and cellular responses.

This study aims to establish the optimal frequency parameters for LICU stimulation and to explore the correlation between spheroid mortality and the volumetric as well as topological changes observed under specific experimental conditions.
The rationale behind this approach is to determine whether frequency-based mortality in LICU can be effective and correlated with a reduction in spheroid volume, providing additional insights into the mechanisms influencing spheroid dynamics.

Additionally, this analysis aims to prevent scenarios where, despite increased mortality, the spheroid mass expands or diffuses, potentially undermining therapeutic effectiveness. The US testing setup in this experiment was calibrated to deliver ultrasound to 3D cancer spheroids through a water medium. Mortality data were obtained using Calcein AM/PI staining [17–20], while morphological and volumetric changes were analyzed using computer vision tools integrated with advanced imaging techniques.

Although previous research has suggested a link between spheroid volume and mortality [21–23], the interplay between these factors under ultrasound stimulation remains insufficiently understood. This study specifically investigates the correlation between low-intensity continuous ultrasound stimulation (under $3, W/cm^2$) and the evolution of spheroid morphology and volume. Confocal microscopy images were analyzed using computer vision-based morphometric techniques to quantify these changes post-stimulation.

The use of three-dimensional spheroid models has become essential in cancer biology research, as these models replicate key characteristics of solid tumors, including gradients of oxygen, nutrients, and therapeutic agents when incorporated into the study. This work aims to establish a relationship between spheroid mortality and volumetric changes under ultrasound stimulation, focusing on parameters such as volume, jaggedness, and compactness.

Additionally, this study aims to correlate the effects of ultrasound treatment intensity with those observed in a previous protocol [1]. The ultrasound stimulation employed here falls within the category of non-thermal therapeutic ultrasound, consistent with recent advancements in the field. As highlighted in the comprehensive study by O'Reilly et al. on non-thermal therapeutic ultrasound [24], the treatment parameters of this study are well-positioned within the low-intensity range, including pressure levels.

The pressure, voltage and frequency tested in [1] are visually reassumed in Figure 1. In contrast, this study investigates the effects of LICU at greater range of frequencies, enabling a direct comparison between the two protocols.

In the experiments conducted in the study by Dimitri et al. [1], the conclusion was that further investigation was required to determine whether there was potential expansion in the volume of the speroids following stimulation. This work therefore sought not only to test a wider range of frequencies, but also to assess the occurrence of volume expansion.

Commonly employed methods for the analysis of spheroids and their features encompass a variety of techniques. These methods include:

- Brightfield microscopy: Enables high-resolution imaging of spheroid morphology and facilitates real-time observation during the growth phase.
- Confocal microscopy: Allows for three-dimensional visualization through z-stack imaging and enables fluorescence staining, making it possible to visualize molecules or detect differences in cell structures with high specificity.
- Feature assessment technique: These often rely on image segmentation and 3D reconstruction, typically implemented using software tools such as ImageJ, MATLAB, or other dedicated applications. Feature extraction can also be performed using programming languages like Python, leveraging advanced libraries such as OpenCV [25–29].

- Emerging technologies: Optical coherence tomography (OCT) is becoming increasingly popular for its ability to provide non-invasive, high-resolution volumetric measurements [30,31]. These methods are often complemented by quantitative metrics such as spheroid diameter, volume, surface roughness, and compactness, which are essential for understanding the biological and mechanical properties of these structures. Regarding this mechanical property of the pancreas, it would be interesting to investigate how much the healthy and malignant properties of the tissue differ between its native form and the spheroid form. This topic has been studied only in tissue form [32], but some studies have recently been published on single cells [33]. However, there is still a lack of information regarding spheroids, partly because their analysis requires a humid and liquid suspension environment. Additionally, working with Atomic Force Microscopy (AFM) under such conditions is not trivial, as it introduces technical challenges related to stability, resolution, and sample preparation

Together, these methodologies offer a comprehensive toolkit for characterizing spheroids, providing valuable insights into their growth dynamics, structural changes, and responses to experimental treatments.

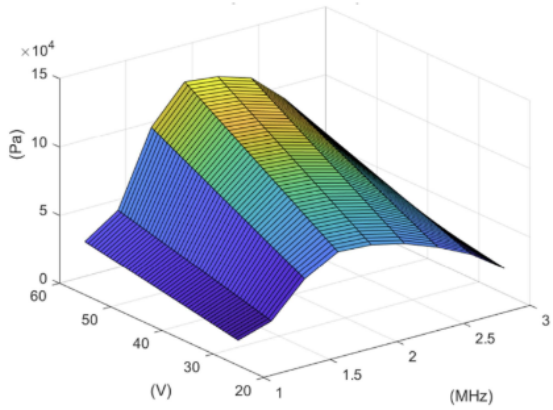

Figure 1. This image shows a 3D representation of pressure, voltage, and frequency levels during the previous stimulation protocol [1], generated using MATLAB from experimental data obtained by HGL200 hydrophone from Honda instruments. This visualization provides an overview of the treatment parameters before the updated protocols. The color changes refer to the peak in the variables intensity.

2. Materials and Methods

2.1. Spheroid Culturing and Staining

Spheroids were cultured using the hanging drop method, a widely recognized technique for three-dimensional cell culture. PANC-1 cells were seeded at a density of 1000 cells per drop in Dulbecco's Modified Eagle Medium (DMEM) supplemented with 10% fetal bovine serum (FBS) and 1% penicillin-streptomycin. The hanging drops were incubated at 37 °C in a 5% CO_2 atmosphere for 48 h to facilitate spheroid formation. Cell viability and mortality within the spheroids were assessed using Calcein AM and Propidium Iodide (PI) staining. Calcein AM labeled live cells with green fluorescence, while PI marked dead cells with red fluorescence. Following minor modifications to the manufacturer's protocol, spheroids were incubated in a staining solution containing 2 µM Calcein AM and 4 µM PI for 30 min at 37 °C before imaging. The total number of samples analyzed, including both treated spheroids and controls, was 256.

2.2. Microscopy and Imaging

Depth-resolved imaging of spheroids was performed using a Zeiss LSM 880 confocal microscope (Carl Zeiss AG, Oberkochen, Germany) equipped with a 20× objective. Z-stack

imaging captured sections with a thickness of 5 µm, with specific channels for Calcein AM (488 nm excitation, 515 nm emission) and PI (561 nm excitation, 617 nm emission). All imaging parameters, including laser power, gain, and exposure time, were kept constant across samples. Calibration beads were employed to verify imaging conditions.

2.3. Ultrasound Stimulation

Spheroids were exposed to low-intensity continuous ultrasound (LICU) stimulation using a function generator (Hantek DSO4102C, Qingdao, China) connected to the trasducer immerged in a tank of degassed water manteined at 34°C to avoid thermal shock in the tridimensional coltures. Two different transducers were used to cover a frequency range from 1 MHz to 5 MHz. The US probes used in the protocol were selected for their central frequency bands: the A307S-SU immersion transducer with a 5 MHz central frequency (Evident Scientific, Waltham, MA, USA) and the WS75-2 transducer (Ultran Group, State College, PA, US). Both transducers are non-focalized cylindrical immersion probes. Uniform energy delivery across samples was ensured using a mechanical two-axis positioning system controlled by Arduino.

2.4. Image Segmentation and Mortality Analysis

Image segmentation and subsequent mortality analysis were carried out using a custom Python-based algorithm, leveraging OpenCV functions [34]. This approach, designed to optimize the segmentation of spheroid confocal images and extract meaningful biological parameters, was implemented through several sequential steps commonly applied in medical image analysis [35–37].

- Image Preprocessing: The original RGB images were converted to grayscale using OpenCV's `cvtColor` function, a standard preprocessing preparatory step that reduces computational complexity while retaining essential information of the image [38,39]. Gaussian blurring was then applied to suppress noise and enhance the precision of subsequent steps. This denoising technique is critical in many image processing applications, particularly in biological imaging, where noise reduction is essential for accurate segmentation [40,41].
- Thresholding: A thresholding procedure was applied to the grayscale image using a method already present in the OpenCV library. This process is a common technique for isolating objects from the background, which is essential in imaging tasks such as cell segmentation [36,42,43]. Pixels below the average grayscale level were set to white, effectively isolating the spheroid and creating a binary representation for further analysis.
- Edge Detection and Contour Identification: The edges of the binary mask were first detected using the Canny edge detection algorithm [44,45]. This algorithm identifies areas of the image where there is a sharp contrast in pixel intensity, essentially outlining the boundaries of objects. Following this, the OpenCV findContours function was used to detect the shapes or contours formed by these edges. Among the detected contours, the largest one, assumed to correspond to the spheroid, was selected and stored for further analysis.
- Mask binary generation and removal of the background of the original confocal color image: A binary mask was obtained by overlaying the detected contour onto a black background using the OpenCV drawContours function. This resulted in an image where the contour was white (255) and the background black (0). The binary mask was then applied to the original color image; this operation performed a pixel-wise logical AND between the binary mask and the color image, effectively isolating and displaying only the region corresponding to the spheroid, while all other areas were set to black.

3. Mortality Analysis

The segmented images with the removal of the background as in Figure 2 were analyzed to assess cell viability. The area of the spheroid was determined by counting the white pixels in the binary mask using the countNonZero function, which provides the total number of pixels within the spheroid region.

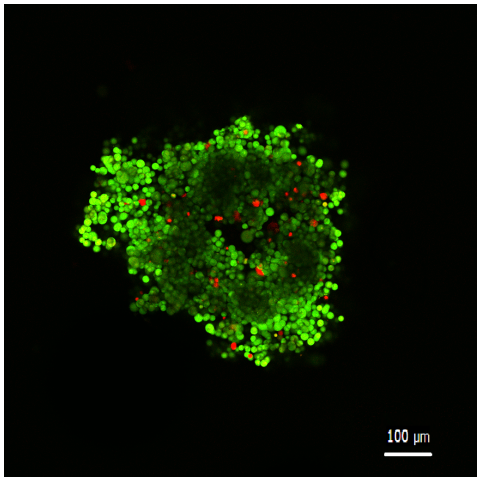

Figure 2. This image obtained by confocal microscopy shows how the Calecin/PI stained image with the background removal appears. The red color is due to PI staining while the green color is due to calcein staining, indicating the mortality and the viability of the single cells.

Subsequently, the ratio of red pixels (representing Propidium Iodide-stained cells) to the total pixels within the spheroid area was calculated. This ratio, indicative of apoptotic cells, was used to quantify the effects of ultrasound treatment, providing insights into cell mortality rates within the treated spheroids. The normalization to the spheroid area was performed to ensure the results were not absolute but relative to the size of the samples, accounting for the natural variability in dimensions observed in biological specimens.

4. Depth-Resolved Mortality Analysis

To study the variation of cell mortality along the spheroid's depth, confocal microscopy Z-stack images were processed. The Figure 3 shows how the spheroid appears on the three sections from the Z-stack. The algorithm was adapted to analyze each image slice individually, enabling the reconstruction of mortality profiles as a function of depth. Furthermore, the advanced version of the segmentation script automatically indexed the slices, streamlining the integration of depth-specific data into the overall statistical analysis.

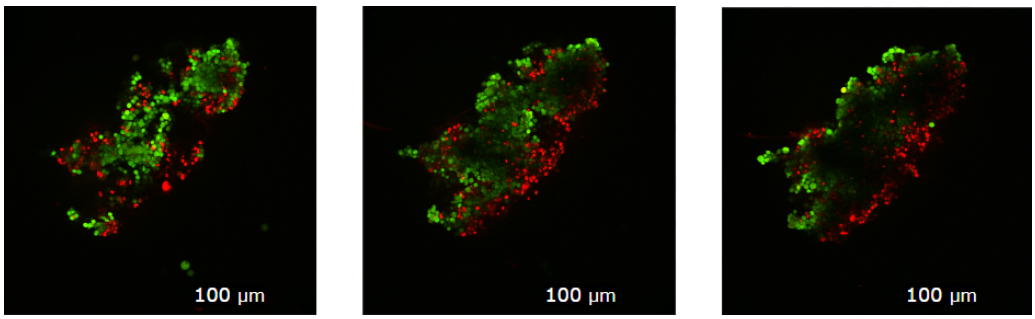

Figure 3. This figure collects the three section from the Z-stack derivate from the same spheroid. The red color is due to PI staining while the green color i due to calcein staining, indicating the mortality and the viability of the single cells.

5. Volume and Disgregation Index Estimation

The volume of spheroids, measured in voxels, was estimated using the ReViSP software tool [46] integrated in the AnaSP 3.0 open source tool [47]. This tool generates 3D volume reconstructions based on the cross-sectional areas of segmented binary masks derived from Z-stack images processed with custom Python scripts. A graphical representation of the steps described in this section is provided in Figure 4.

The volume of each spheroid was calculated using segmented binary masks. To account for biological variability, the volumes of treated spheroids were subjected to a weighted average relative to the volumes of untreated control spheroids from the same experimental day. This normalization step minimized variability caused by biological differences between samples, ensuring more reliable comparisons. For each treatment frequency, the mean volume of all treated spheroids was computed, allowing for the correlation of volume changes with cell mortality at specific frequencies.

5.1. Morphological Analysis and Disgregation Index

The perimeter-to-area ratio of each spheroid's cross-sectional image was calculated to assess morphological changes. This metric, referred to as the disgregation index, provides a measure of spheroid border irregularity. The disgregation index was evaluated separately for treated and untreated spheroids to determine the extent of cellular dispersion induced by ultrasound (US) excitation. This dispersion may have adverse outcomes, including the potential promotion of metastasis [48–52].

For statistical data analysis, the perimeter-to-area ratios were averaged within each frequency group for both treated and control samples. A ratio of these averages (treated versus control) was calculated to evaluate the impact of treatment on the disgregation index, while accounting for biological variability. Area and perimeter measurements were obtained using AnaSP [53], an open source tool designed for spheroid analysis, with segmented images of the spheroids used as input.

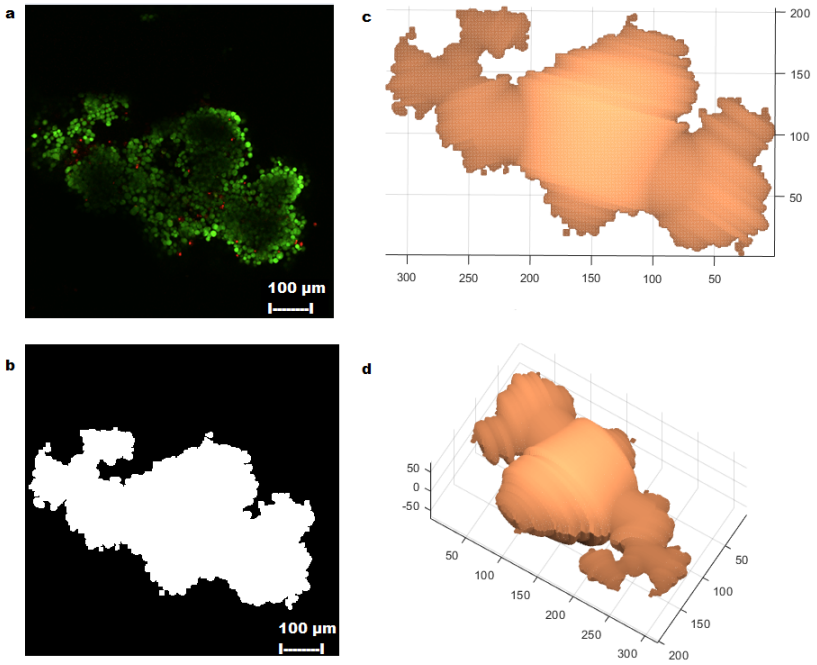

Figure 4. Steps to derive the volume evalutaion: how the varius steps appear graphically (**a**); the confocal image with Calcein/PI staining (**b**); the segmentation and binary mask (**c**); top view from ReVisp graphical interface (**d**), a side view of the volume is visible.

For the disgregation index, statistical analysis was performed by first averaging the ratios for each frequency across both treated and control groups. Then, a ratio of these averages was calculated to evaluate changes in the disgregation index introduced by treatment, while accounting for biological variability.

5.2. Software and Code Availability

AnaSP and ReViSP, two open-source tools, are now integrated into the AnaSP 3.0 open-source framework, which can be accessed via their respective repositories [46,47,53]. Additionally, custom Python scripts developed for segmentation of cofocal images and analysis are available upon request from the corresponding author.

6. Results

The analysis of spheroids subjected to LICU revealed significant correlations between treatment frequency, as shown in Figure 5, and tumor volume reduction, illustrated in Figure 6. Finally, the spheroid disgregation index is displayed in Figure 7. Data were gathered across frequencies of 1 MHz to 5 MHz for the mortality analysis, for the volume and disgregation index we only focused on the range from 2 MHz to 4 MHz. The focus on a narrower range was motivated by the results of the mortality analyses. Specifically, the most significant findings were observed between 2 MHz and 4 MHz, where two distinct peaks in mortality were identified: one at 2 MHz and another, of varying magnitude, at 3.5 MHz.

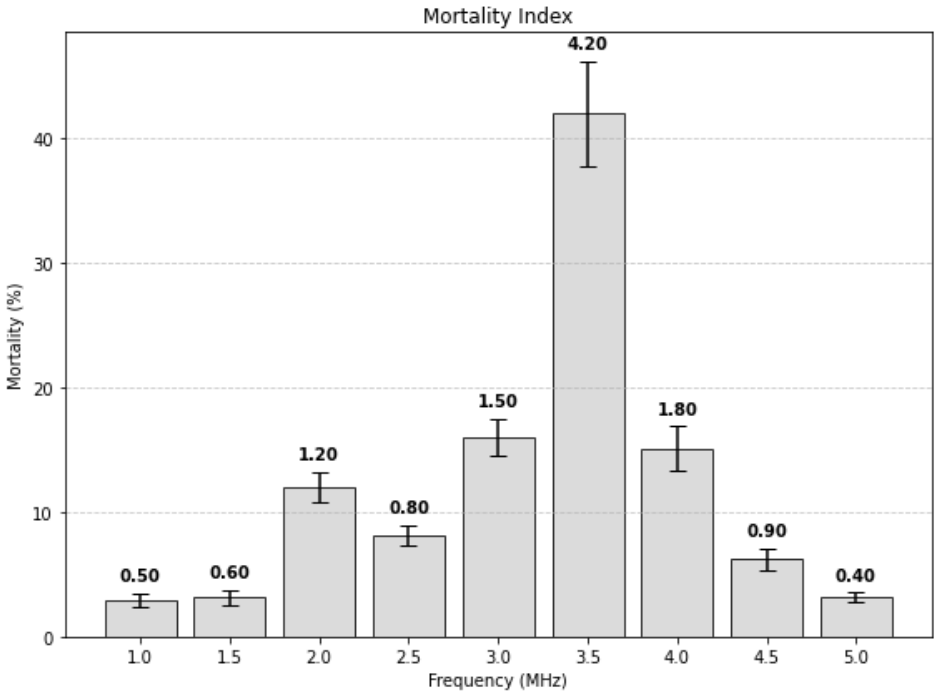

Figure 5. The mortality ratio obtained by evaluating the PI-stained pixels weighted on the spheroid's segmented area. The standard deviation is also displayed for each histogram column.

In the volume histogram, intensity values around 1 indicate that the volume remains unchanged, neither expanding nor contracting. Similarly, in the disaggregation histogram, values close to 1 suggest that the spheroids neither disaggregate nor expand. These values are highlighted in bold in the Figures 6 and 7.

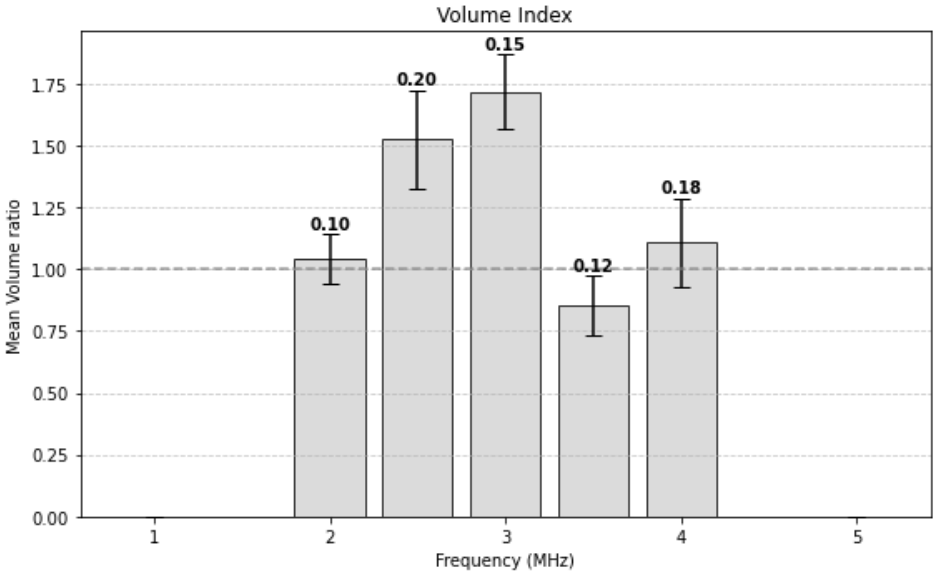

Figure 6. The volume mean ratio obtained by making the evaluation of treated Volume on Control volume. The standard deviation is also displayed for each histogram column.

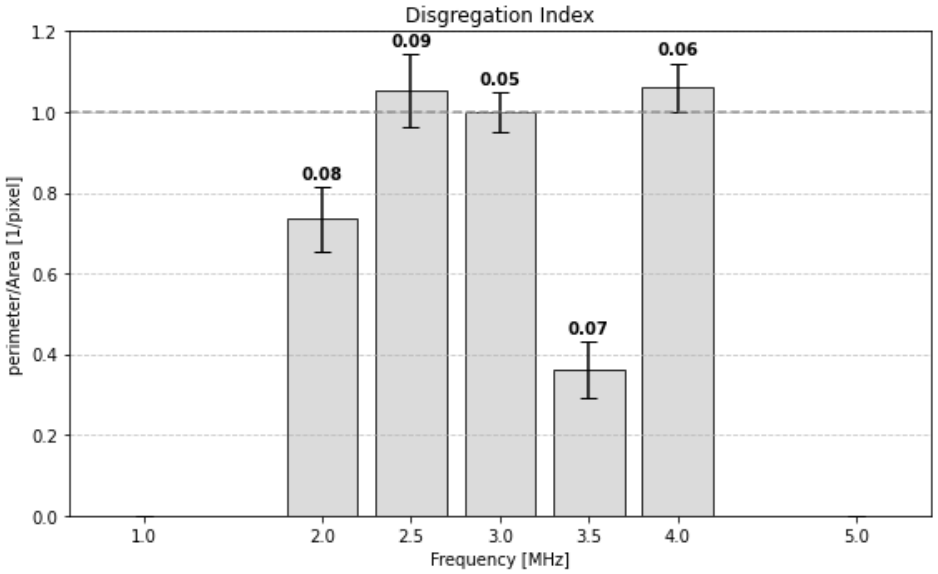

Figure 7. The disgregation index is obtained by making the evaluation of the mean treated perimeter on area on the mean control perimeter on area. The standard deviation is also displayed for each histogram column.

7. Discussion

The results indicate a strong correlation between LICU treatment at specific frequencies and the observed changes in spheroid behavior, as demonstrated in Figure 6.

At a frequency of 2 MHz, a substantial reduction in spheroid volume was recorded. This effect was accompanied by a smaller peak in mortality rates, as depicted in Figure 5, alongside a noticeable decrease in the disgregation index (Figure 7).

Such findings suggest that LICU at 2 MHz induces measurable alterations in three-dimensional spheroid cultures. These observations hint at the potential for off-target effects at 2 MHz, which may influence spheroid architecture without completely compromising cell viability.

In contrast, the effects observed at 3.5 MHz were particularly striking. This frequency was associated with a marked increase in mortality rates, as illustrated in Figure 5, coupled with a marked reduction in the volume of the spheroid (Figure 6).

Furthermore, there is a significant decrease in the disgregation index (Figure 7) at 3.5 MHz underscores. Unlike the effects at 2 MHz, treatment at 3.5 MHz appeared to cause higher mortality rates, still preventing disaggregation.

This distinction is crucial, as excessive disgregation could facilitate metastasis, a concern supported by the literature that highlights the mechanical and structural consequences of spheroid disaggregation [48–51].

Thus, LICU at 3.5 MHz demonstrates a dual capability: it induces significant cellular mortality while promoting spheroid destabilization, with potential implications for therapeutic strategies targeting tumor cohesion and survival.

These findings highlight the nuanced interplay between frequency-specific LICU effects on spheroids. Although 2 MHz elicits subtle structural changes with limited mortality, 3.5 MHz emerges as a more potent frequency to cause cell death, potentially offering a targeted approach to therapeutic interventions. Future investigations should focus on further elucidating the mechanistic underpinnings of these frequency-dependent effects, with an emphasis on optimizing therapeutic windows to balance efficacy and safety.

The following section provides a concise yet comprehensive statistical analysis of the data presented in the figures. This analysis aims to assess the significance of the observed differences and to identify the correlations.

Regarding the mortality data it is noted that the sample size exceeds 250 and the p value is significantly less than 0.05.

Regarding the statistical analysis of the indices, the standard deviation of the volume index is consistently below 0.2, indicating relatively low variability. The statistical correlation values derived from the volume index suggest a significant relationship with mortality.

Specifically, the volume index shows a correlation coefficient of -0.496, indicating a correlation. The corresponding t-score is -3.023 and the p-value for this result is 0.0053, which is well below the commonly used significance threshold of 0.05. This confirms that the correlation is statistically significant and suggests that changes in volume index may be related to mortality.

For the disgregation index, the standard deviation is smaller, remaining below 0.09, suggesting even less variability in these measurements.

This index shows a stronger negative correlation with mortality, with a correlation coefficient of -0.800. The t-score is -7.052. The corresponding p-value is 1.14×10^{-7}, which is extremely small, indicating an exceptionally strong and statistically significant relationship.

The statistical analysis reveals that both the volume index and the disgregation index show significant correlations with mortality. Both indices have p-values well below 0.05, confirming their statistical significance.

These findings suggest that both indices are relevant factors in understanding mortality. Therefore, it indicates that mortality is statistically correlated with the morphological changes detected by the computer vision analysis conducted.

All statistical evaluations were performed using Google Sheets and Python.

At this stage, a comparison with similar studies is essential. The following section provides a review of relevant research.

Bazou et al. [2] published a study in 2017 investigating the effects of LICU treatment. Their findings indicate that continuous low-intensity ultrasound (LICU) increases the levels of pro-inflammatory cytokines IFN-γ, IL-1β, and TNF-α in murine pancreatic tumors without inducing significant thermal, mechanical, or structural alterations. These results

suggest that LICU has the potential to modulate the tumor inflammatory response, which could lead to additional anti-tumor effects.

More recently, in 2023, González et al. [14] demonstrated that LICU significantly inhibits the migration of PANC-1 cells in vitro. This finding suggests that LICU could play a role in limiting the spread of cancer cells.

In 2022, Song et al. [54] proposed a mechanistic explanation for the efficacy of low-intensity ultrasound, supported by both in vitro and in vivo experiments. Their study focuses on the mechanosensitive Piezo1 channel as a potential therapeutic target for pancreatic ductal adenocarcinoma (PDAC). Piezo1 is a membrane protein that responds to mechanical stimuli, such as pressure changes, by facilitating calcium (Ca^{2+}) influx into the cell. This calcium signaling regulates key biological processes, including apoptosis, which is critical for cancer therapy.

The results show that Piezo1 is highly expressed in pancreatic cancer cells compared to healthy tissue. The experiments used ultrasound combined with microbubbles (US + MB), a non-invasive technique that uses microbubble oscillations to generate localised mechanical stimuli. This combination activates Piezo1, causing an increase in intracellular calcium and mitochondrial dysfunction, which in turn induces tumour cell apoptosis.

It is important to note that while there is evidence to suggest a correlation between the Piezo1 cation channel and the induction of cell death by LICU, the underlying mechanisms responsible for the observed effectiveness at 3.5 MHz and the secondary peak at 2 MHz remain to be fully elucidated. It is therefore plausible that these phenomena may not be attributable to a single, shared biological rationale.

These studies are closely related to the work presented in this publication, further confirming the results obtained in the experiments. However, certain aspects require further clarification, both in existing literature and in future research involving the use of LICU in the pancreas. Specifically, additional studies on in vivo applications are necessary, along with more comparative tests using healthy cells to validate the selectivity of the treatment.

8. Conclusions

The findings demonstrate that mortality peaks coincide with significant spheroid shrinkage. Moreover, the correlation with the reduced disgregation index highlights the need for further investigation, building on the team's previous work [1], which emphasized the importance of excluding potential disgregation caused by LICU. The simultaneous reduction in volume and mortality at 2 and 3.5 MHz frequencies suggests a therapeutic balance where LICU achieves maximum efficiency in targeting tumor spheroids while minimizing the risks of disgregation. Notably, the decrease in the disgregation index at these critical frequencies further supports LICU's efficacy, indicating an optimal mechanism that compromises tumor cohesion without promoting cellular dispersion. The ultimate goal of this work is to gain a deeper understanding of the effectiveness of LICU. Demonstrating selectivity through in vitro testing on healthy pancreatic cells, along with further validation of its efficacy in murine models inoculated with human PDAC, could significantly enhance the technology readiness level and move this technology closer to feasibility for human treatments. Furthermore, it would be highly valuable to investigate the behavior of the Piezo1 cationic channel during stimulation, focusing on its activation dynamics and the role of calcium ion flux, to provide greater insight into the mechanistic pathways involved and refine the therapeutic strategy. These steps are considered crucial for advancing the research and bringing the technology closer to clinical application.

Despite the promising results obtained, certain limitations must be addressed to further advance the clinical applicability of LICU. One major challenge is the lack of commercially available ultrasonic amplifiers capable of continuously amplifying ultrasound waves for

biomedical applications. Currently, the only available solutions are designed for civil and seismic engineering, necessitating the development of a customized system optimized for therapeutic use. Additionally, translating the stinolation protocol to in vivo models presents significant technical hurdles. Water, commonly used as a coupling medium in in vitro experiments, is a difficult fitting option for in vivo applications, necessitating the identification of a biocompatible and echogenic coupling material. Overcoming these limitations will be essential for refining the therapeutic approach and bridging the gap between preclinical validation and potential clinical translation.

Author Contributions: Conceptualization, M.D. and A.C.; methodology, A.C.; software, M.R. and M.S.; validation M.D. and A.C; formal analysis, M.R.; investigation, M.R.; resources, M.D. and A.C.; data curation, M.R.; writing—original draft preparation, M.R.; writing—review and editing, M.R. and A.C.; visualization, M.R.; supervision, M.D. and A.C.; project administration, A.C. and M.D.; funding acquisition, A.C. and M.D. All authors have read and agreed to the published version of the manuscript.

Funding: Financial support from the Italian Ministry of University and Research (PNRR projects "AGE-IT—Ageing well in an ageing society") is gratefully acknowledged.

Institutional Review Board Statement: Ethical review and approval were not required for this study, as confirmed by the Ethical Committee for Animal Experimentation of the University of Florence. The study exclusively involved commercially available cell lines (PANC-1 spheroids) and did not include live animals or patient-derived samples.

Data Availability Statement: The Python code is available upon request from the corresponding author.

Acknowledgments: The authors wish to acknowledge Annarosa Arcangeli and Claudia Duranti, Jessica Iorio, and Chiara Capitani for providing the cell cultures and for their valuable suggestions.

Conflicts of Interest: The authors declare no conflicts of interest.

References

1. Dimitri, M.; Duranti, C.; Aquino, S.; Mazzantini, L.; Iorio, J.; Lulli, M.; Ricci, M.; Capineri, L.; Arcangeli, A.; Corvi, A. Biophysical and Biomechanical Effect of Low Intensity US Treatments on Pancreatic Adenocarcinoma 3D Cultures. *Appl. Sci.* **2022**, *12*, 666. [CrossRef]
2. Bazou, D.; Maimon, N.; Munn, L.L.; Gonzalez, I. Effects of low intensity continuous ultrasound (LICU) on mouse pancreatic tumor explants. *Appl. Sci.* **2017**, *7*, 1275. [CrossRef]
3. Maloney, E.; Hwang, J.H. Emerging HIFU applications in cancer therapy. *Int. J. Hyperth.* **2015**, *31*, 302–309. [CrossRef] [PubMed]
4. Barkin, J. High intensity focused ultrasound (HIFU). *Can. J. Urol.* **2011**, *18*, 5634.
5. Haar, G.T. HIFU Tissue Ablation: Concept and Devices. In *Therapeutic Ultrasound*; Escoffre, J.M., Bouakaz, A., Eds.; Springer: Cham, Switzerland, 2016; pp. 3–20.
6. Feril, L.B.; Kondo, T. Biological effects of low intensity ultrasound: The mechanism involved, and its implications on therapy and on biosafety of ultrasound. *J. Radiat. Res.* **2004**, *45*, 479–489. [CrossRef]
7. Wood, A.K.; Sehgal, C.M. A review of low-intensity ultrasound for cancer therapy. *Ultrasound Med. Biol.* **2015**, *41*, 905–928. [CrossRef] [PubMed]
8. Fraldi, M.; Cugno, A.; Deseri, L.; Dayal, K.; Pugno, N. A frequency-based hypothesis for mechanically targeting and selectively attacking cancer cells. *J. R. Soc. Interface* **2015**, *12*, 20150656. [CrossRef]
9. Loria, R.; Giliberti, C.; Bedini, A.; Palomba, R.; Caracciolo, G.; Ceci, P.; Falvo, E.; Marconi, R.; Falcioni, R.; Bossi, G.; et al. Very low intensity ultrasounds as a new strategy to improve selective delivery of nanoparticles-complexes in cancer cells. *J. Exp. Clin. Cancer Res.* **2019**, *38*, 1–11. [CrossRef] [PubMed]
10. Ricci, M.; Barbi, E.; Dimitri, M.; Duranti, C.; Arcangeli, A.; Corvi, A. Sonoporation, a Novel Frontier for Cancer Treatment: A Review of the Literature. *Appl. Sci.* **2024**, *14*, 515. [CrossRef]
11. Zhang, K.; Xu, H.; Chen, H.; Jia, X.; Zheng, S.; Cai, X.; Wang, R.; Mou, J.; Zheng, Y.; Shi, J. CO_2 bubbling-based'nanobomb'system for targetedly suppressing panc-1 pancreatic tumor via low intensity ultrasound-activated inertial cavitation. *Theranostics* **2015**, *5*, 1291. [CrossRef]

12. Kuo, Y.Y.; Chen, W.T.; Lin, G.B.; Lu, C.H.; Chao, C.Y. Study on the effect of a triple cancer treatment of propolis, thermal cycling-hyperthermia, and low-intensity ultrasound on PANC-1 cells. *Aging* **2023**, *15*, 7496. [CrossRef] [PubMed]
13. Qiu, F.; Chen, J.; Cao, J.; Diao, F.; Huang, P. Low-intensity low-frequency ultrasound enhances the chemosensitivity of gemcitabine-resistant ASPC-1 cells via PI3K/AKT/NF-κB pathway-mediated ABC transporters. *Oncol. Rep.* **2020**, *44*, 1158–1168. [CrossRef]
14. González, I.; Luzuriaga, J.; Valdivieso, A.; Candil, M.; Frutos, J.; López, J.; Hernández, L.; Rodríguez-Lorenzo, L.; Yagüe, V.; Blanco, J.L.; et al. Low-intensity continuous ultrasound to inhibit cancer cell migration. *Front. Cell Dev. Biol.* **2023**, *10*, 842965. [CrossRef] [PubMed]
15. Lagneaux, L.; de Meulenaer, E.C.; Delforge, A.; Dejeneffe, M.; Massy, M.; Moerman, C.; Hannecart, B.; Canivet, Y.; Lepeltier, M.F.; Bron, D. Ultrasonic low-energy treatment: A novel approach to induce apoptosis in human leukemic cells. *Exp. Hematol.* **2002**, *30*, 1293–1301. [CrossRef]
16. Amaya, C.; Luo, S.; Baigorri, J.; Baucells, R.; Smith, E.R.; Xu, X.X. Exposure to low intensity ultrasound removes paclitaxel cytotoxicity in breast and ovarian cancer cells. *BMC Cancer* **2021**, *21*, 1–13. [CrossRef] [PubMed]
17. Dong, G.; Wang, S.; Ge, Y.; Deng, Q.; Cao, Q.; Wang, Q.; Shang, Z.; OuYang, W.; Li, J.; Liu, C.; et al. Serum-free culture system for spontaneous human mesenchymal stem cell spheroid formation. *Stem Cells Int.* **2019**, *2019*, 6041816. [CrossRef]
18. Kiyomi, A.; Miyakawa, R.; Matsumoto, J.; Yamazaki, K.; Imai, S.; Yuan, B.; Hirano, T.; Sugiura, M. Potent antitumor activity of cepharanthine against triple-negative breast cancer spheroids compared with tetrandrine. *Oncol. Lett.* **2020**, *20*, 331. [CrossRef] [PubMed]
19. Singh, S.K.; Abbas, S.; Saxena, A.K.; Tiwari, S.; Sharma, L.K.; Tiwari, M. Critical role of three-dimensional tumorsphere size on experimental outcome. *Biotechniques* **2020**, *69*, 333–338. [CrossRef] [PubMed]
20. Kessel, S.; Cribbes, S.; Déry, O.; Kuksin, D.; Sincoff, E.; Qiu, J.; Chan, L.L.Y. High-throughput 3D tumor spheroid screening method for cancer drug discovery using celigo image cytometry. *Slas Technol. Transl. Life Sci. Innov.* **2017**, *22*, 454–465. [CrossRef]
21. Yeon, S.E.; No, D.Y.; Lee, S.H.; Nam, S.W.; Oh, I.H.; Lee, J.; Kuh, H.J. Application of concave microwells to pancreatic tumor spheroids enabling anticancer drug evaluation in a clinically relevant drug resistance model. *PLoS ONE* **2013**, *8*, e73345. [CrossRef]
22. Dinter, J.; Friedrich, R.P.; Yang, H.; Pilarsky, C.; Mangge, H.; Pöttler, M.; Janko, C.; Alexiou, C.; Lyer, S. Mitoxantrone and mitoxantrone-loaded iron oxide nanoparticles induce cell death in human pancreatic ductal adenocarcinoma cell spheroids. *Materials* **2023**, *16*, 2906. [CrossRef] [PubMed]
23. Maftouh, M.; Avan, A.; Sciarrillo, R.; Granchi, C.; Leon, L.G.; Rani, R.; Funel, N.; Smid, K.; Honeywell, R.; Boggi, U.; et al. Synergistic interaction of novel lactate dehydrogenase inhibitors with gemcitabine against pancreatic cancer cells in hypoxia. *Br. J. Cancer* **2014**, *110*, 172–182. [CrossRef] [PubMed]
24. O'Reilly, M.A. Exploiting the mechanical effects of ultrasound for noninvasive therapy. *Science* **2024**, *385*, eadp7206. [CrossRef] [PubMed]
25. Li, G.; Zhang, Y.; Xu, B.; Li, X. Image analysis and processing of skin cell injury based on OpenCV. *J. Phys. Conf. Ser.* **2019**, *1237*, 032003. [CrossRef]
26. Meimban, R.J.; Fernando, A.R.; Monsura, A.; Rañada, J.; Apduhan, J. Blood cells counting using python OpenCV. In Proceedings of the 2018 14th IEEE International Conference on Signal Processing (ICSP), Piscataway, NJ, USA, 12–16 August 2018; Volume 144, pp. 50–53.
27. Khan, A.A. Tuberculosis: Image Segmentation Approach Using OpenCV. *Sukkur IBA J. Comput. Math. Sci.* **2018**, *2*, 1–7.
28. Ojeme, B.; Quinn, F.; Karls, R.; Quinn, S. Fully Automated Methods for the Detection and Segmentation of Mitochondria in Microscopy Images. *Int. J. Mech. Mater. Eng.* **2023**, *17*, 42–47.
29. Bui, M.Q.V.; Ngo, D.T.; Pham, H.A.; Nguyen, D.D. GAC3D: Improving monocular 3D object detection with ground-guide model and adaptive convolution. *PeerJ Comput. Sci.* **2021**, *7*, e686. [CrossRef]
30. Huang, Y.; Zou, J.; Badar, M.; Liu, J.; Shi, W.; Wang, S.; Guo, Q.; Wang, X.; Kessel, S.; Chan, L.L.Y.; et al. Longitudinal morphological and physiological monitoring of three-dimensional tumor spheroids using optical coherence tomography. *J. Vis. Exp. JoVE* **2019**, *144*, e59020. [CrossRef]
31. Sharma, M.; Verma, Y.; Rao, K.; Nair, R.; Gupta, P. Imaging growth dynamics of tumour spheroids using optical coherence tomography. *Biotechnol. Lett.* **2007**, *29*, 273–278. [CrossRef] [PubMed]
32. Pagnanelli, M.; De Gaetano, F.; Callera, A.; Nappo, G.; Capretti, G.; Carrara, S.; Ferrari, A.M.R.; Cellesi, F.; Costantino, M.L.; Zerbi, A. Analysis of the Mechanical Characteristics of Human Pancreas through Indentation: Preliminary In Vitro Results on Surgical Samples. *Biomedicines* **2024**, *12*, 91. [CrossRef] [PubMed]
33. Nguyen, A.V.; Nyberg, K.D.; Scott, M.B.; Welsh, A.M.; Nguyen, A.H.; Wu, N.; Hohlbauch, S.V.; Geisse, N.A.; Gibb, E.A.; Robertson, A.G.; et al. Stiffness of pancreatic cancer cells is associated with increased invasive potential. *Integr. Biol.* **2016**, *8*, 1232–1245. [CrossRef]
34. Bradski, G.; Kaehler, A. *Learning OpenCV: Computer Vision with the OpenCV Library*; O'Reilly Media, Inc.: Sebastopol, CA, USA, 2008.
35. Haidekker, M. *Advanced Biomedical Image Analysis*; John Wiley & Sons: Hoboken, NJ, USA, 2010.

36. Altun, A.A.; Taghiyev, A. Advanced image processing techniques and applications for biological objects. In Proceedings of the 2017 2nd IEEE International Conference on Computational Intelligence and Applications (ICCIA), Piscataway, NJ, USA, 8–11 September 2017, pp. 340–344.
37. Merchant, F.; Castleman, K. *Microscope Image Processing*; Academic Press: Cambridge, MA, USA, 2022.
38. Sarfraz, M. Introductory Chapter: On Digital Image Processing. In *Digital Imaging*; IntechOpen: London, UK, 2020.
39. Gonzalez, R.C. *Digital Image Processing*; Pearson Education India: Chennai, India, 2009.
40. Gedraite, E.S.; Hadad, M. Investigation on the effect of a Gaussian Blur in image filtering and segmentation. In Proceedings of the ELMAR-2011, Zadar, Croatia, 14–16 September 2011; pp. 393–396.
41. Kumar, N.; Nachamai, M. Noise removal and filtering techniques used in medical images. *Orient. J. Comput. Sci. Technol* **2017**, *10*, 103–113. [CrossRef]
42. Gençtav, A.; Aksoy, S.; Önder, S. Unsupervised segmentation and classification of cervical cell images. *Pattern Recognit.* **2012**, *45*, 4151–4168. [CrossRef]
43. Mir, M.A.; Qazi, F.; Naseem, M.; Zia, S.S.; Mubeen, T. Invisibility Cloak using Color Extraction and Image Segmentation with OpenCV. In Proceedings of the 2022 Global Conference on Wireless and Optical Technologies (GCWOT), Malaga, Spain, 14–17 February 2022; pp. 1–6.
44. Luo, Y.; Duraiswami, R. Canny edge detection on NVIDIA CUDA. In Proceedings of the 2008 IEEE Computer Society Conference on Computer Vision and Pattern Recognition Workshops, Anchorage, AL, USA, 23–28 June 2008; pp. 1–8.
45. Punagin, A.; Punagin, S. Analysis of lane detection techniques on structured roads using OpenCV. *Int. J. Res. Appl. Sci. Eng. Technol.* **2020**, *8*, 2994–3003. [CrossRef]
46. Piccinini, F.; Peirsman, A.; Stellato, M.; Pyun, J.c.; Tumedei, M.M.; Tazzari, M.; De Wever, O.; Tesei, A.; Martinelli, G.; Castellani, G. Deep learning-based tool for morphotypic analysis of 3D multicellular spheroids. *J. Mech. Med. Biol.* **2023**, *23*, 2340034. [CrossRef]
47. Stellato, M.; Rydzyk, M.M.; Pannella, M.; Rossi, F.; Cappadone, C.; Remondini, D.; Pyun, J.C.; Normanno, N.; Ibrahim, T.; Castellani, G.; et al. Radiomic analysis of 3D spheroids using 2D brightfield images. *Biomed. Signal Process. Control.* **2025**, *103*, 107366. [CrossRef]
48. McKenzie, A.J.; Hicks, S.R.; Svec, K.V.; Naughton, H.; Edmunds, Z.L.; Howe, A.K. The mechanical microenvironment regulates ovarian cancer cell morphology, migration, and spheroid disaggregation. *Sci. Rep.* **2018**, *8*, 7228. [CrossRef]
49. Zhang, Q.; Lin, F.; Huang, J.; Xiong, C. Mechanical transmission enables EMT cancer cells to drive epithelial cancer cell migration to guide tumor spheroid disaggregation. *Sci. China Life Sci.* **2022**, *65*, 2031–2049. [CrossRef] [PubMed]
50. Burleson, K.M.; Boente, M.P.; Pambuccian, S.E.; Skubitz, A.P. Disaggregation and invasion of ovarian carcinoma ascites spheroids. *J. Transl. Med.* **2006**, *4*, 1–16. [CrossRef]
51. Nawrocki Raby, B.; Polette, M.; Gilles, C.; Clavel, C.; Strumane, K.; Matos, M.; Zahm, J.M.; Van Roy, F.; Bonnet, N.; Birembaut, P. Quantitative cell dispersion analysis: New test to measure tumor cell aggressiveness. *Int. J. Cancer* **2001**, *93*, 644–652. [CrossRef]
52. Pinto, B.; Henriques, A.C.; Silva, P.M.; Bousbaa, H. Three-dimensional spheroids as in vitro preclinical models for cancer research. *Pharmaceutics* **2020**, *12*, 1186. [CrossRef] [PubMed]
53. Piccinini, F.; Tesei, A.; Arienti, C.; Bevilacqua, A. Cancer multicellular spheroids: Volume assessment from a single 2D projection. *Comput. Methods Programs Biomed.* **2015**, *118*, 95–106. [CrossRef] [PubMed]
54. Song, Y.; Chen, J.; Zhang, C.; Xin, L.; Li, Q.; Liu, Y.; Zhang, C.; Li, S.; Huang, P. Mechanosensitive channel Piezo1 induces cell apoptosis in pancreatic cancer by ultrasound with microbubbles. *iScience* **2022**, *25*, 103733. [CrossRef] [PubMed]